Article in Press

Mode conversion of hyperbolic phonon polaritons in van der Waals terraces

Byung-Il Noh, Sina Jafari Ghalekohneh, Mingyuan Chen, Jialiang Shen, Eli Janzen, Lang Zhou, Pengyu Chen, James H. Edgar, Bo Zhao & Siyuan Dai

We are providing an unedited version of this manuscript to give early access to its findings. Before final publication, the manuscript will undergo further editing. Please note there may be errors present which affect the content, and all legal disclaimers apply.

If this paper is publishing under a Transparent Peer Review model then Peer Review reports will publish with the final article.

Mode Conversion of Hyperbolic Phonon Polaritons in van der Waals terraces

Byung-Il Noh[1†], Sina Jafari Ghalekohneh[2†], Mingyuan Chen[1], Jialiang Shen[1], Eli Janzen[3], Lang Zhou[1], Pengyu Chen[1], James Edgar[3], Bo Zhao[2]*, and Siyuan Dai[1]*

[1]*Materials Research and Education Center, Department of Mechanical Engineering, Auburn University, Auburn, Alabama 36849, USA*

[2]*Department of Mechanical Engineering, University of Houston, Houston, Texas, 77204, USA*

[3]*Tim Taylor Department of Chemical Engineering, Kansas State University, Manhattan, Kansas 66506, USA*

*Correspondence to: sdai@auburn.edu and bzhao8@uh.edu

[†]These authors contribute equally

Abstract

Electromagnetic hyperbolicity has driven key functionalities in nanophotonics, including super-resolution imaging, efficient energy control, and extreme light manipulation. Central to these advances are hyperbolic polaritons—nanometer-scale light-matter waves—spanning multiple energy-momentum dispersion orders with distinct mode profiles and incrementally high optical momenta. In this work, we report the mode conversion of hyperbolic polaritons across different dispersion orders by breaking the structure symmetry in engineered step-shape van der Waals (vdW) terraces. The mode conversion from the fundamental to high-order hyperbolic polaritons is imaged using scattering-type scanning near-field optical microscopy (s-SNOM) on both hexagonal boron nitride (hBN) and alpha-phase molybdenum trioxide (α-MoO$_3$) vdW terraces. Our s-SNOM data, augmented with electromagnetics simulations, further demonstrate the alteration of polariton mode conversion by varying the step size of vdW terraces. The mode conversion reported here offers a practical approach toward integrating previously independent different-order hyperbolic polaritons with ultra-high momenta, paving the way for promising applications in nano-optical circuits, sensing, computation, information processing, and super-resolution imaging.

Introduction

Electromagnetic hyperbolicity[1], characterized by opposite signs in the principal components of the permittivity tensor ($\varepsilon_i\varepsilon_j < 0$, where $i, j = x, y$ or z), drives important advances in nanophotonics. These include the exceptionally high photonic density of states, unconventional light propagation, and access to deep sub-diffraction optics. Such advances have led to valuable functionalities like super-resolution imaging[2-4], efficient energy control[5-8], and extreme light manipulation[9, 10]. At the core of these advances and functionalities are high-momentum (high-k) hyperbolic polaritons—the nanometer-scale light-matter waves confined in hyperbolic materials. Following the Fabry-Pérot resonance condition[11], hyperbolic polaritons span multiple energy-momentum (ω-k) dispersion branches (Figure 1a, indexed by $l = 0, 1, 2, \ldots$) with incremental momenta k and distinct mode profiles. These different-order hyperbolic polaritons can be studied using far-field Fourier Transform Infrared Spectroscopy on nano-patterned hyperbolic materials[12-14]. Real-space near-field studies typically image the lowest-k zeroth-order ($l = 0$) hyperbolic polaritons as dominant single-period polariton fringes[11, 15-23]. Two recent works on alpha-phase molybdenum trioxide (α-MoO_3)[24, 25] reveal high-order ($l > 0$) hyperbolic polaritons using geometric confinement at specific frequencies[24] and strong near-fields in nanowires[25], both of which directly launch high-order polaritons. In isotopically pure hBN[26], reduced phonon loss enables direct imaging of high-order polariton fringes. While different-order hyperbolic polaritons have been probed, their distinct momenta and mode profiles make them relatively independent, lacking evident interaction, integration, or conversion.

In this work, we report mode conversions of different-order hyperbolic polaritons (e.g., arrow, Figure 1a) by breaking structure symmetry in van der Waals (vdW) terraces with engineered step-shape edges. These mode conversions result from changes in polariton momentum k upon reflection at asymmetric step-shape edges, in contrast to conventional symmetric simple slab edges that tend to preserve both momentum and mode profile during reflection. Moreover, the mode conversions of different-order hyperbolic polaritons can be altered by varying the step sizes at the asymmetric edges. Our combined experimental and theoretical results uncover the distinct nano-optical phenomenon of polariton mode conversions by simple vdW engineering. The mode conversion offers a practical approach towards integrating previously independent different-order hyperbolic polaritons with ultra-high momenta for advanced polariton nano-optical functionalities.

Results

Nano-imaging of polariton mode conversion in vdW terraces

The mode conversions between different-order hyperbolic polaritons were revealed through infrared nano-imaging of engineered vdW terraces using the scattering-type scanning near-field optical microscopy (s-SNOM, Figure 1d). Hexagonal boron nitride (hBN) terraces were assembled using the pickup-and-stack technique[27] from mechanically exfoliated vdW thin slabs (Figures 1b-c). It features both simple slab edges, where the sample completely terminates (Figure 1e, bottom), and step-shape edges, where the sample partially terminates on the top part, forming a step (Figure 1e, top). The characterization tool s-SNOM is an illuminated atomic force microscope (AFM) that simultaneously records topography and nano-optical images of the underneath sample (Figure 1d). The s-SNOM observable near-field amplitude S_3 (methods) with a spatial resolution of ~ 10 nm can map nano-optical phenomena in real space. On polaritonic materials, the s-SNOM tip acts as an antenna[28] to bridge the momentum mismatch and transfer energy between free-space light (wavelength λ_f and frequency $\omega = 1/\lambda_f$) and polaritons[15, 16].

In the hBN terraces, hyperbolic polaritons are imaged close to the simple slab edges and step-shape edges. At the simple slab edge (Figure 1d, black dashed box), parallel fringes were

observed, similar to previous s-SNOM works on polaritons[11, 15-19]. They show the strongest oscillation closest to the edge, followed by damped ones away from the edge, as evidenced in the s-SNOM line profile as a function of the distance to the edge L (Figure 2a, black curve). Fourier Transform (FT) analysis (Figure 2b) of the line profile from the simple slab edge reveals two evident resonances at $\Delta = 3$ and 6 μm^{-1}. They correspond to the standing wave interferences between the edge-launched polaritons and the free-space illumination and the interferences between the tip-launched and edge-reflected polaritons, respectively[29]. A systematic s-SNOM study at various ω reveals the ω-k polariton dispersion along the zeroth-order ($l = 0$) hyperbolic branch, as verified by our calculation in Figure 2e. Briefly, hyperbolic polaritons span multiple ω-k dispersion branches[11]:

$$k = k_l' + ik_l'' = -\frac{\Psi}{d}[\arctan\left(\frac{1}{\varepsilon_t\Psi}\right) + \arctan\left(\frac{\varepsilon_s}{\varepsilon_t\Psi}\right) + \pi l], \ \Psi = \frac{\sqrt{\varepsilon_z}}{i\sqrt{\varepsilon_t}}, \quad (1)$$

where d is the hBN thickness, $l = 0, 1, 2, 3, \ldots$ is an integer and the branch index (mode order). ε_s is the substrate permittivity, $\varepsilon_t = \varepsilon_x = \varepsilon_y$ and ε_z are the in-plane and out-of-plane permittivities of hBN. $k = k_l' + ik_l''$ is the complex in-plane momentum of hyperbolic polaritons and relates to the polariton wavelength λ_l by $k_l' = 2\pi / \lambda_l$.

While the data at hBN simple slab edges align with conventional s-SNOM studies[11, 15-23] to probe hyperbolic polaritons mainly at the zeroth-order, our results at the step-shape edges (Figure 1d, red dashed boxes) reveal distinct characteristics. In addition to the relatively long-period polariton fringes observed at simple slab edges, short-period beats superimposed on these fringes appear near a variety of step-shaped edges. These step-shaped edges include both regular and covered steps (Figure 1f, red boxes). As shown in the s-SNOM line profiles (red and blue curves in Figure 2a), these short-period beats decay from the step-shape edges into the sample interior, similar to the long-period fringes. The FT spectra in Figures 2c-d reveal evident resonances $\Delta = 35$ μm^{-1} for these beats. They correspond to standing waves with a wavelength much smaller than the zeroth-order ($l = 0$) hyperbolic polaritons.

In hyperbolic materials, the observed short-period beats are indicative of high-order ($l > 0$) hyperbolic polaritons. However, due to their short propagation length and high k (see Eq. 1)[11], standard tip-launch-edge-reflect and edge-launch-photon-interfere mechanisms do not produce evident interference for high-order hyperbolic polaritons, as evidenced by our data at the simple slab edge (Figure 2b) and previous works[11, 15-23]. Instead, the short-period beats are predominantly attributed to the mode conversion of hyperbolic polaritons from the zeroth-order branch to the high-order branches (arrow, Figure 1a) when the former was launched by the tip, propagated, and reached the step-shape edges. Specifically, hyperbolic phonon polaritons propagate inside the vdW slab following a zigzag trajectory by reflecting at the top and bottom surfaces. Upon reaching a simple slab edge (Figure 1e, bottom), these polaritons reflect off the vertical sidewall without evident scattering, thereby preserving their original mode order and profile. In contrast, a step-shape edge (Figure 1e, top) introduces a sharp step corner that can strongly scatter[22, 30] the incoming polaritons inside the slab. This scattering provides additional momentum[22, 30], enabling mode conversion by bridging the k-mismatch between polaritons of different orders. As a result, zeroth-order ($l = 0$) polaritons are converted into first-order ($l = 1$) modes upon reflection at the step-shaped edge. In our experiment, these converted $l = 0 \rightarrow 1$ first-order polaritons propagate back towards the s-SNOM tip and interfere with the newly launched $l = 0$ polaritons, forming standing wave interferences between the tip and the step-shape edge (see detailed analysis of the interference mechanism in Supplementary Note 1). As the sample is scanned underneath the tip, the standing wave interference is recorded as short-period beats in our s-SNOM image (Figure 1d).

Notably, high-order hyperbolic polaritons exhibit much shorter propagation lengths than their zeroth-order counterpart. Therefore, without the mode conversion, it is difficult for high-order polaritons to complete a tip-launch-edge-reflect round trip to produce evident standing wave interferences at either simple slab edges (Figure 1d black box and ref. [11, 15-23]) or step-shape edges. Note that weak signals around 65 μm^{-1}—by its value, may correspond to the tip-launch-edge-reflect $l = 1$ polariton fringes—cannot correlate with dominant s-SNOM signatures, especially the $l = 0 \rightarrow 1$ beats (see the FT decomposition of our s-SNOM data in Supplementary Note 2).

The observed mode conversion is corroborated in the ω-k dispersion of hyperbolic polaritons (Figures 2f-g). The standing wave interference between the converted first-order and the newly launched zeroth-order polaritons produces a periodic resonance of $\Delta = k_0' + k_1'$ (Supplementary Note 1). Therefore, the momentum k_1' of the converted $l = 0 \rightarrow 1$ hyperbolic polaritons can be extracted from the FT spectra in Figures 2c-d. These extracted s-SNOM data (red and blue dots) from both the step-shape edge and the covered step-shape edge reveal a systematic ω dependence and agree well with our ω-k dispersion calculation (false color maps) in Figures 2f-g, thereby validating the polariton mode conversion mechanism described above.

Polariton mode conversion induced by asymmetric step-shape edges is expected to be generic to hyperbolic materials featuring multiple ω-k dispersion branches. In Figure 3, we studied this effect in terraces made of another representative hyperbolic vdW material, α-MoO_3. The α-MoO_3 terraces were fabricated using the similar pickup-and-stack technique[27] as for hBN (Figure 1). The s-SNOM amplitude images of a simple slab α-MoO_3 (Figure 3a) and a terraced α-MoO_3 with a step-shape edge (Figure 3b) exhibit distinct features. Consistent with the results in hBN (Figures 1–2), long-period polariton fringes are observed near the edge of the simple slab (Figure 3a). In contrast, near the step-shaped edge (Figure 3b), short-period beats are superimposed on these fringes, indicating the polariton mode conversion. FT analysis of the s-SNOM line profiles (Figures 3c–d) reveals clear signatures of the $l = 0 \rightarrow 1$ mode conversion at the step-shaped edge (Figure 3f). The extracted momentum k_1' (red dots, Figure 3h) shows excellent agreement with the ω-k dispersion calculation (false color map, Figure 3h).

Numerical simulation to verify the polariton mode conversion

In order to further verify the polariton mode conversion phenomenon, we carried out total-field scattered-field electromagnetic simulations using the Finite Difference Frequency Domain (FDFD) method (see details in Supplementary Note 3). We calculated the electric field E_x at the cross-sections of the simple slab and step-shape hBN terraces (Figures 4e and 4g). Hyperbolic polaritons are launched from the black dashed lines and propagate along the $+x$ direction. Different orders of hyperbolic polaritons show distinct mode profiles (Figures 4a-d) following their Fabry-Pérot resonances indexed by l[11, 31]. They possess different symmetries and are either even ($l = 0$, 2, …) or odd ($l = 1$, 3, …) to the hBN slab centerline. Upon reaching the edges, these polaritons get reflected, propagate along the $-x$ direction, and are finally analyzed at the left side of the source, where the polariton reflectivity at various branches can be extracted using mode orthogonality. These FDFD simulations support our experimental results by revealing that edge symmetry is crucial in polariton mode conversion. During the reflection, while the symmetric simple slab edge preserves polaritons in the same order (same l), the asymmetric step-shape edge does not, leading to strong mode conversion. For example, in hBN structures, input from our experiments in Figure 1, zero-order ($l = 0$) hyperbolic polaritons are launched before the simple slab and step-shaped edges. The FT results reveal that the simple slab edge mainly reflects these polaritons into the zeroth order (Figure 4f). In contrast, the step-shape edge reflects them into both the zeroth and the first order (Figure 4h), indicating an evident $l = 0 \rightarrow 1$ polariton mode conversion. In Figures 4i-j,

we quantify the mode conversion rate using reflectivity R_{ij}—the power ratio between the reflected j-th order mode due to the incident i-th order mode—for more generalized cases where the incident hyperbolic polaritons are at $l = 0, 1, 2$, and 3. Notably, the symmetric simple slab edge preserves the polariton modal symmetry (Figure 4i): R_{00}, R_{11}, R_{22}, and R_{33} are significantly larger than others, indicating that even (odd) modes $l = 0, 2, \dots$ (1, 3, …) are only reflected into even (odd) modes. Conversely, the asymmetric step-shape edge reflects polaritons into both odd and even modes, regardless of the order of the incident polaritons (Figure 4j)—demonstrating that breaking edge symmetry leads to polariton mode conversion.

Altering the polariton mode conversion in vdW terraces

After demonstrating the mode conversion of hyperbolic polaritons at asymmetric step-shape edges, we investigate the alteration of mode conversion by varying the step size. In Figure 5, we study the polariton mode conversion in hBN terraces where all thicker sides of their step-shape edges have identical thicknesses $H = 51$ nm, but thinner sides have different thicknesses h. Figures 5b-c present representative s-SNOM images of these hBN terraces with thinner side thicknesses $h = 17$ and 34 nm ($h/H = 0.33$ and 0.67). The clear differences in the imaged polariton fringes and beats in Figures 5b and 5c suggest a strong dependence of mode conversion on the step size. This trend is further revealed by the s-SNOM line profiles (Figure 5d) and the extracted $l = 0 \to 1$ polariton line profiles from the inverse FT analysis (Figure 5e, more details about the FT analysis are provided in Supplementary Note 4). Among all the terraces studied, the one with $h/H = 0.33$ exhibits the strongest $l = 0 \to 1$ oscillation (red profile). Since all incident zeroth-order (tip-launched) hyperbolic polaritons are identical (Figure 5a, all $H = 51$ nm), the terrace with a step-shape edge of $h/H = 0.33$ yields the highest $l = 0 \to 1$ mode conversion rate R_{01}. For both smaller and larger h/H, the converted first-order polariton oscillations are weaker, corresponding to lower $l = 0 \to 1$ mode conversion rates R_{01}. The mode conversion rate R_{01} can be quantified by measuring the oscillation amplitude of the converted $l = 0 \to 1$ polariton line profiles[32, 33]. In Figure 5f, we plot the dependence of the mode conversion rate on the step ratio h/H (see details in Supplementary Note 5), where the experimental data from the s-SNOM imaging (squares) agree excellently with the FDFD simulation results (curve).

Discussion

Combined s-SNOM nano-imaging data, electromagnetics modeling, and FDFD simulations in Figures 1–5 demonstrate the mode conversion of hyperbolic polaritons in vdW terraces. The mode conversion originates from the strong scattering at asymmetric step-shape edges that bridges the momentum mismatch and transfers the energy between hyperbolic polaritons across different-order dispersion branches. The observed different-order polariton mode conversion can be altered by varying the step size in the terraced structures. Therefore, the mode conversion demonstrated in our work provides a practical approach toward integrating previously independent different-order hyperbolic polaritons with ultra-high momentum and precious figures of merit for advanced polariton nano-optical functionalities. Future works may be directed toward tailoring edges or implementing metastructures at the edges for on-demand polariton mode conversion and propagation redirection[34] at specific orders. The polariton mode conversion may be varied by delicately controlling the steepness of the asymmetric edges (Supplementary Note 6). In addition, polariton launchers may be implemented on one side of the vdW terrace to study the polariton transmission and mode conversion across the step-shape edges. Moreover, it is worth integrating the mode conversion structures into practical nano-optical devices for nano-optical

circuits, sensing, computation, energy transfer, information processing, and super-resolution imaging.

During the manuscript peer review process, we became aware of a related study reporting boundary-excited high-order hyperbolic phonon polaritons and the pseudo-birefringence effect in α-MoO$_3$[37].

Methods
Fabrication of vdW terraces

The hBN and α-MoO$_3$ terraces featuring simple slab and step-shape edges were assembled using the standard vdW dry transfer method. hBN and α-MoO$_3$ bulk crystals were grown using Cr–Fe flux with a temperature gradient[35] and thermal physical vapor deposition[36]. The vdW slabs were mechanically exfoliated from bulk crystals and transferred onto Si wafers with 300 nm thick thermal oxide. Using a poly (bisphenol A carbonate)/polydimethylsiloxane stamp, vdW terraces were assembled by partially picking up the exfoliated large vdW slab and stacking that part on top of the original slab.

Infrared nano-imaging

The infrared nano-imaging of hyperbolic polariton mode conversion in the terraced vdW was conducted using the scattering-type scanning near-field optical microscope (s-SNOM, www.neaspec.com). The s-SNOM is based on a tapping-mode atomic force microscope (AFM). The PtIr coated AFM tip with a radius of ~ 10 nm (Arrow-NCPt, NanoWorld AG, Switzerland) was illuminated by monochromatic Mid-IR quantum cascade lasers (QCLs, www.daylightsolutions.com) with frequency spanning 845 to 1800 cm^{-1}. The nano-IR s-SNOM images were recorded by a pseudoheterodyne interferometric detection module with a tapping frequency of 245–280 kHz and tapping amplitude of ~ 70 nm. The detected optical signal was demodulated at the third harmonics (S_3) of the tapping frequency in order to obtain the pure near-field signal.

Data Availability

Relevant data supporting the key findings of this study are available within the article and the Supplementary Information file. All raw data generated during the current study are available from the corresponding authors upon request.

References:

1. Poddubny, A., Iorsh, I., Belov, P. & Kivshar, Y. Hyperbolic metamaterials. *Nature Photonics* **7**, 948 (2013).
2. Dai, S. et al. Subdiffractional focusing and guiding of polaritonic rays in a natural hyperbolic material. *Nature Communications* **6**, 6963 (2015).
3. Li, P. et al. Hyperbolic phonon-polaritons in boron nitride for near-field optical imaging and focusing. *Nature Communications* **6**, 7507 (2015).
4. Liu, Z., Lee, H., Xiong, Y., Sun, C. & Zhang, X. Far-Field Optical Hyperlens Magnifying Sub-Diffraction-Limited Objects. *Science* **315**, 1686-1686 (2007).
5. Krishnamoorthy, H.N.S., Jacob, Z., Narimanov, E., Kretzschmar, I. & Menon, V.M. Topological Transitions in Metamaterials. *Science* **336**, 205 (2012).

6. Lu, D., Kan, J.J., Fullerton, E.E. & Liu, Z. Enhancing spontaneous emission rates of molecules using nanopatterned multilayer hyperbolic metamaterials. *Nature Nanotechnology* **9**, 48-53 (2014).

7. Jacob, Z., Smolyaninov, I.I. & Narimanov, E.E. Broadband Purcell effect: Radiative decay engineering with metamaterials. *Applied Physics Letters* **100**, 181105 (2012).

8. Tielrooij, K.-J. et al. Out-of-plane heat transfer in van der Waals stacks through electron–hyperbolic phonon coupling. *Nature Nanotechnology* **13**, 41-46 (2018).

9. Li, P. et al. Infrared hyperbolic metasurface based on nanostructured van der Waals materials. *Science* **359**, 892-896 (2018).

10. Li, P. et al. Collective near-field coupling and nonlocal phenomena in infrared-phononic metasurfaces for nano-light canalization. *Nature Communications* **11**, 3663 (2020).

11. Dai, S. et al. Tunable Phonon Polaritons in Atomically Thin van der Waals Crystals of Boron Nitride. *Science* **343**, 1125-1129 (2014).

12. Nandanwar, S. et al. Determining the optical and polaritonic properties of isotopically pure hBN using cryogenic FTIR micro-spectroscopy. *Applied Physics Letters* **126** (2025).

13. Gubbin, C.R., De Liberato, S. & Folland, T.G. Surface phonon polaritons for infrared optoelectronics. *Journal of Applied Physics* **131** (2022).

14. Caldwell, J.D. et al. Sub-diffractional volume-confined polaritons in the natural hyperbolic material hexagonal boron nitride. *Nature Communications* **5**, 5221 (2014).

15. Low, T. et al. Polaritons in layered two-dimensional materials. *Nature Materials* **16**, 182 (2016).

16. Basov, D.N., Fogler, M.M. & García de Abajo, F.J. Polaritons in van der Waals materials. *Science* **354**, aag1992 (2016).

17. Chen, M. et al. Van der Waals isotope heterostructures for engineering phonon polariton dispersions. *Nature Communications* **14**, 4782 (2023).

18. Hu, G., Shen, J., Qiu, C.-W., Alù, A. & Dai, S. Phonon Polaritons and Hyperbolic Response in van der Waals Materials. *Advanced Optical Materials* **8**, 1901393 (2020).

19. Wang, H. et al. Planar hyperbolic polaritons in 2D van der Waals materials. *Nature Communications* **15**, 69 (2024).

20. Xu, X.G. et al. One-dimensional surface phonon polaritons in boron nitride nanotubes. *Nature Communications* **5**, 4782 (2014).

21. Shi, Z. et al. Amplitude- and Phase-Resolved Nanospectral Imaging of Phonon Polaritons in Hexagonal Boron Nitride. *ACS Photonics* **2**, 790-796 (2015).

22. Yoxall, E. et al. Direct observation of ultraslow hyperbolic polariton propagation with negative phase velocity. *Nature Photonics* **9**, 674 (2015).

23. Ni, G. et al. Long-Lived Phonon Polaritons in Hyperbolic Materials. *Nano Letters* **21**, 5767-5773 (2021).

24. He, M. et al. Guided Polaritons along the Forbidden Direction in MoO_3 with Geometrical Confinement. *Nano Letters* **23**, 5035-5041 (2023).

25. Lu, G. et al. Launching and Manipulation of Higher-Order In-Plane Hyperbolic Phonon Polaritons in Low-Dimensional Heterostructures. *Advanced Materials* **35**, 2300301 (2023).

26. Giles, A.J. et al. Ultralow-loss polaritons in isotopically pure boron nitride. *Nature Materials* **17**, 134 (2017).

27. Kim, K. et al. van der Waals Heterostructures with High Accuracy Rotational Alignment. *Nano Letters* **16**, 1989-1995 (2016).

28. Atkin, J.M., Berweger, S., Jones, A.C. & Raschke, M.B. Nano-optical imaging and spectroscopy of order, phases, and domains in complex solids. *Advances in Physics* **61**, 745-842 (2012).

29. Dai, S. et al. Efficiency of Launching Highly Confined Polaritons by Infrared Light Incident on a Hyperbolic Material. *Nano Letters* **17**, 5285-5290 (2017).

30. Huber, A., Ocelic, N., Kazantsev, D. & Hillenbrand, R. Near-field imaging of mid-infrared surface phonon polariton propagation. *Applied Physics Letters* **87**, 081103 (2005).

31. Kumar, A., Low, T., Fung, K.H., Avouris, P. & Fang, N.X. Tunable Light–Matter Interaction and the Role of Hyperbolicity in Graphene–hBN System. *Nano Letters* (2015).

32. Dai, S.Y. et al. Hyperbolic Phonon Polaritons in Suspended Hexagonal Boron Nitride. *Nano Letters* **19**, 1009-1014 (2019).

33. Woessner, A. et al. Highly confined low-loss plasmons in graphene-boron nitride heterostructures. *Nature Materials* **14**, 421-425 (2015).

34. Wu, Y. et al. Monolithically Structured van der Waals Materials for Volume-Polariton Refraction and Focusing. *ACS Nano* **18**, 17065-17074 (2024).

35. Li, J. et al. Hexagonal Boron Nitride Single Crystal Growth from Solution with a Temperature Gradient. *Chemistry of Materials* **32**, 5066-5072 (2020).

36. Wang, Y. et al. Growth of Large-Scale, Large-Size, Few-Layered α-MoO_3 on SiO_2 and Its Photoresponse Mechanism. *ACS Applied Materials & Interfaces* **9**, 5543-5549 (2017).

37. Chen, N. et al. Boundary-induced excitation of higher-order hyperbolic phonon polaritons. *Nature Photonics* **19**, 1225–1232 (2025).

Author contributions: S. D. conceived the idea. B. -I. N., M. C., and J. S. fabricated the device and performed the optical experiments. L. Z. assisted with the plasma cleaning of the substrates for the van der Waals terraces. E. J. and J. E. provided the hBN crystals. S. J. G. and B. Z. conducted the theory and simulations. B. -I. N., S. D., S. J. G., and B. Z. analyzed the data. S. D., B. Z., J. E., and P. C. supervised the project.
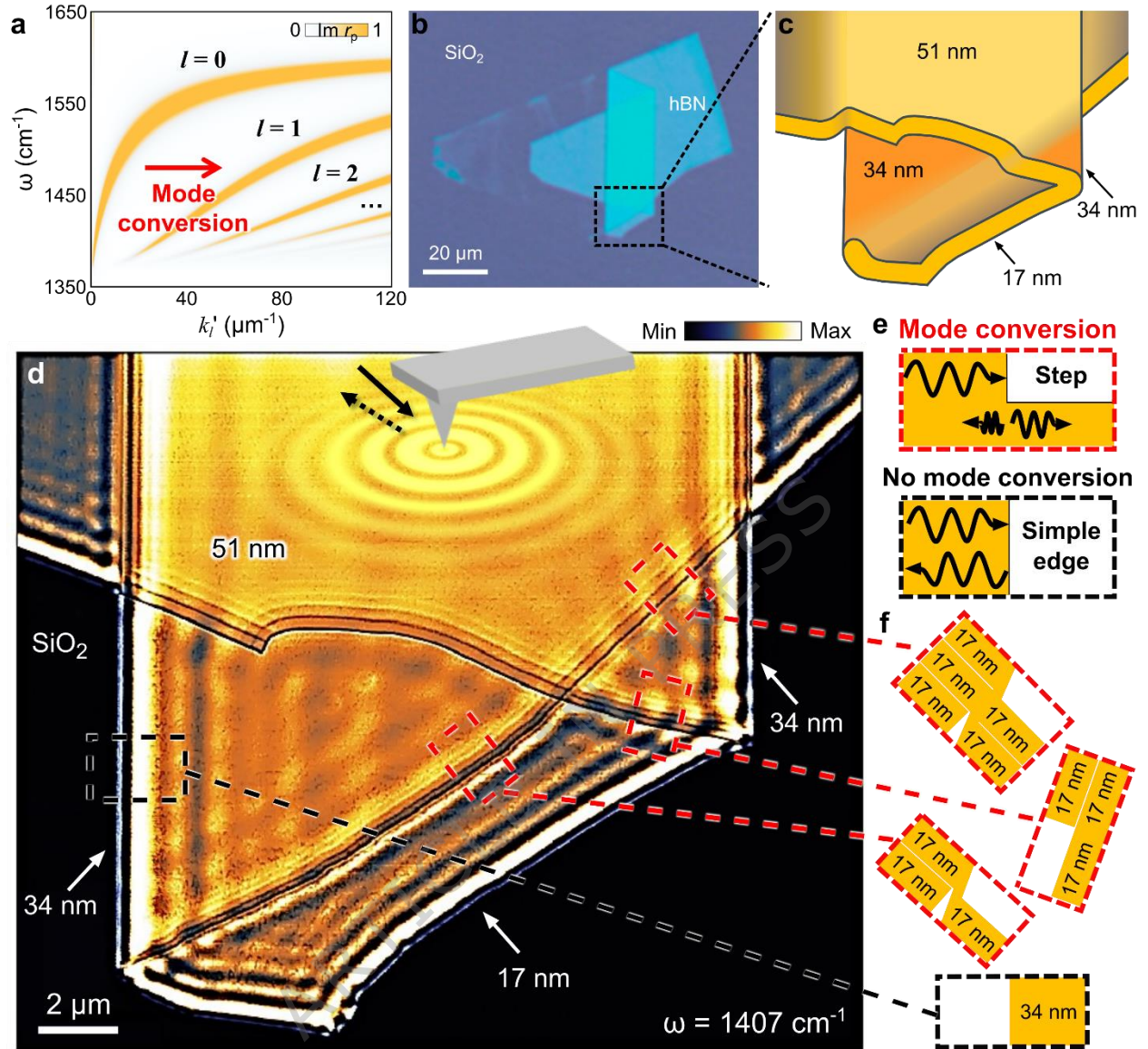
Figure 1 | Nano-infrared imaging of hyperbolic phonon polariton mode conversion in the hexagonal boron nitride (hBN) terrace using scattering-type scanning near-field optical microscopy (s-SNOM). **a**, The energy-momentum (ω-k) dispersion of hyperbolic phonon polaritons in hBN (thickness: 34 nm) shown as a false-color map calculated by the imaginary part of the reflecivity, Im(r_p). The red arrow indicates the mode conversion of the zeroth-order ($l = 0$) hyperbolic polariton into high-order ($l = 1, 2, \cdots$) hyperbolic polaritons. **b**, The optical microscope image of terraced hBN made by the pickup-and-stack technique from a mechanically exfoliated hBN thin slab. **c**, The schematic of the hBN terrace featuring a variety of simple slab, step, and covered step edges. **d**, s-SNOM amplitude image of the terraced hBN at the infrared (IR) frequency $\omega = 1407$ cm^{-1}. The solid and dotted black arrows represent the incident and backscattered IR light at the s-SNOM tip (grey). The concentric orange circles delineate the hyperbolic phonon polariton waves launched by the s-SNOM tip in the terraced hBN. **e**, Schematics of mode conversion and no mode conversion of hyperbolic phonon polaritons at the step-shape edge (top) and the simple

slab edge (bottom), respectively. **f,** Cross-section schematics of the step-shape edges (top) and simple slab edge (bottom) in (**d**).
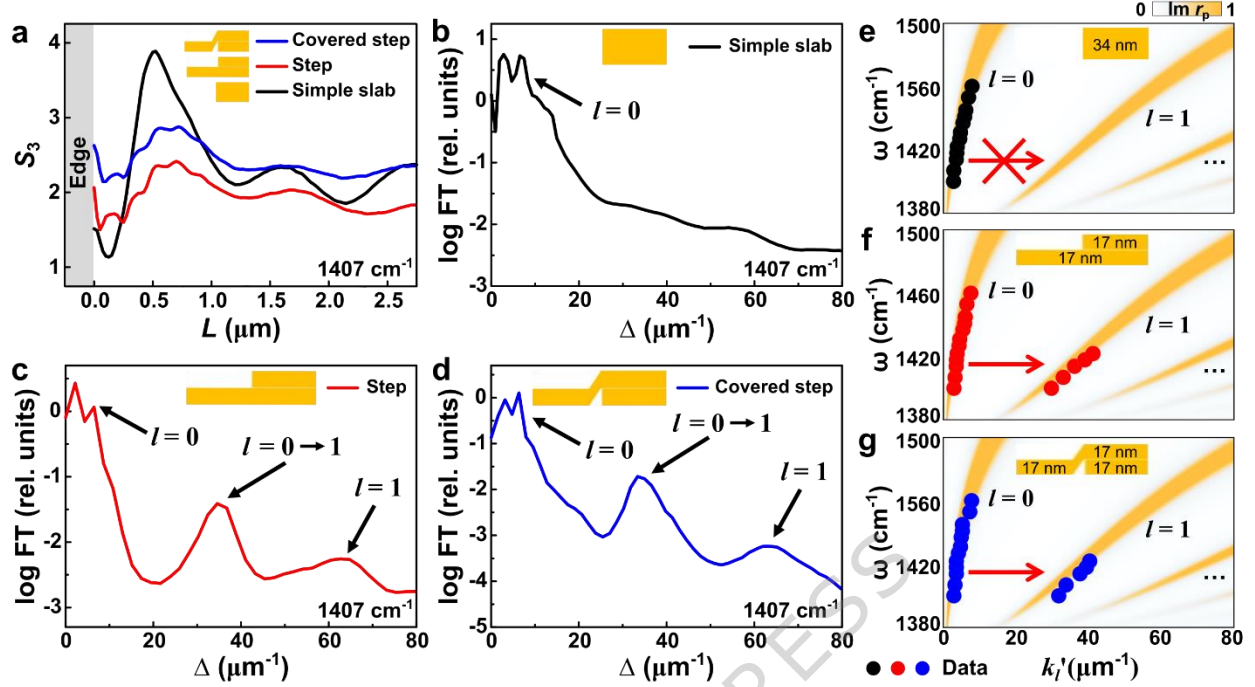
Figure 2 | s-SNOM line profiles and energy-momentum (ω-*k*) dispersions of hyperbolic phonon polaritons at various edges in the hBN terrace. a, s-SNOM line profiles taken from simple slab and step-shape edges in Figure 1d. **b–d,** Fourier transform (FT) spectra of the s-SNOM line profiles from the symmetric simple slab edge (**b**), asymmetric step-shape edge (**c**), and asymmetric covered step-shape edge (**d**) in Figure 2a. In the simple slab edge (**b**), the FT peaks show zeroth-order hyperbolic phonon polaritons (*l* = 0) features from the standard edge-launch-photon-interference and tip-launch-edge-reflect-interference mechanisms. Unlike the symmetric simple slab edge, the asymmetric step-shape edges (**c** and **d**) reveal high-order hyperbolic phonon polaritons (*l* = 1) from the *l* = 0 → 1 mode conversion. **e–g,** ω-*k* dispersions of hyperbolic phonon polaritons from the simple slab edge (**e**), step-shape edge (**f**), and covered step-shape edge (**g**), respectively. The thicker side thickness of the hBN is 34 nm. The s-SNOM data and simulation results are plotted with dots and false-color maps, respectively.
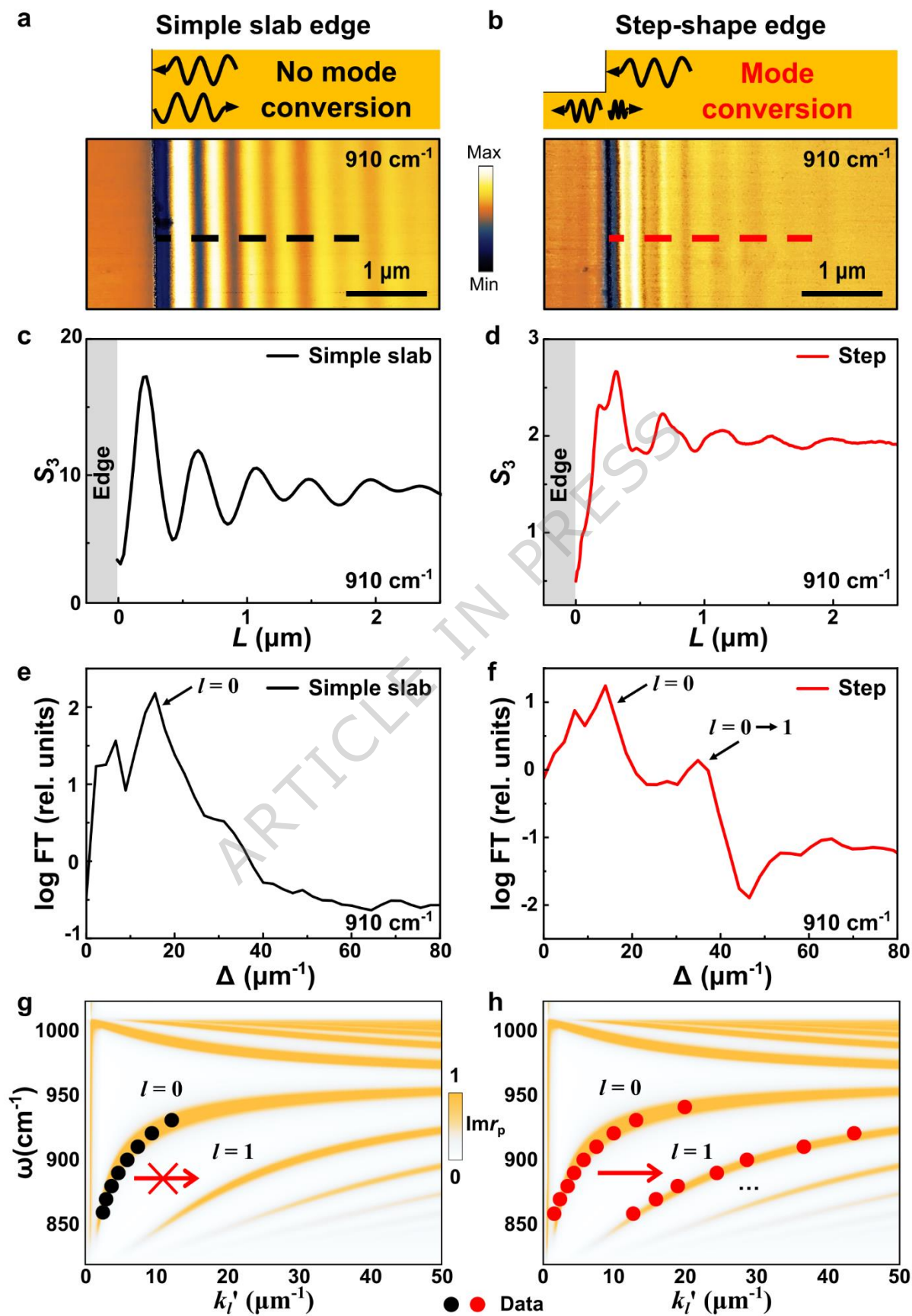
a Simple slab edge — No mode conversion — 910 cm⁻¹ — 1 µm — Max/Min

b Step-shape edge — Mode conversion — 910 cm⁻¹ — 1 µm

c S_3 vs L (µm) — Simple slab — Edge — 910 cm⁻¹

d S_3 vs L (µm) — Step — Edge — 910 cm⁻¹

e log FT (rel. units) vs Δ (µm⁻¹) — $l = 0$ — Simple slab — 910 cm⁻¹

f log FT (rel. units) vs Δ (µm⁻¹) — $l = 0$ — $l = 0 \rightarrow 1$ — Step — 910 cm⁻¹

g ω (cm⁻¹) vs k_l' (µm⁻¹) — $l = 0$ — $l = 1$ — Imr_p 0–1

h ω (cm⁻¹) vs k_l' (µm⁻¹) — $l = 0$ — $l = 1$ — Data

Figure 3 | Mode conversion of hyperbolic phonon polaritons in alpha-phase molybdenum trioxide (α-MoO₃) terraces. a, **b,** Schematics and s-SNOM images of polaritons around the α-MoO₃ simple slab edge (thickness: 160 nm) (**a**) and step-shaped edge (left and right thicknesses = 81 and 165 nm, respectively) (**b**) at $\omega = 910$ cm^{-1}. Unlike the symmetric simple slab edge (**a**), the asymmetric step-shape edge (**b**) of the α-MoO₃ terrace reveals beats indicating a similar hyperbolic polariton mode conversion to those in hBN terraces (Figures 1–2). **c, d,** s-SNOM line profiles extracted from the simple slab (black dashed line) and step-shape (red dashed line) edges in Figures 3a, b. **e, f,** FT spectra of the s-SNOM line profiles from the symmetric simple slab edge and asymmetric step-shape edge in Figures 3c, d. **g, h,** ω-k dispersion of hyperbolic phonon polaritons of α-MoO₃ from the simple slab edge (**g**) and the step-shape edge (**h**). The s-SNOM data and simulation results are plotted with color dots and false-color maps, respectively.
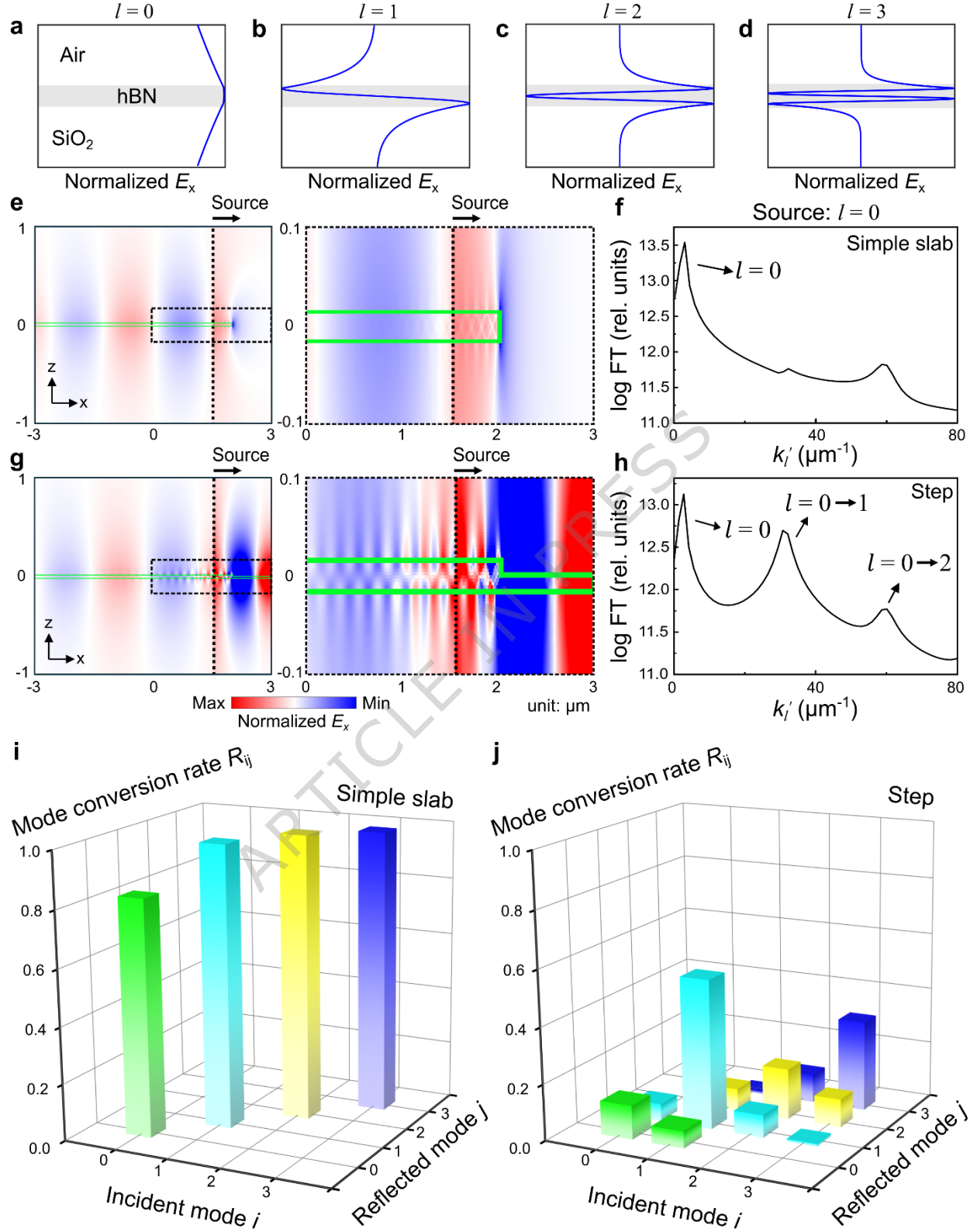
Figure 4 | Finite-difference frequency-domain (FDFD) simulation of hyperbolic polariton mode conversions in the hBN terrace. **a–d,** The normalized *x*-component of electric field (E_x) for (**a**) zeroth-order, (**b**) first-order, (**c**) second-order, and (**d**) third-order hyperbolic phonon

polaritons. **e**, **g,** False color maps of E_x at the cross-sections of the simple slab (symmetric, **e**) and step-shape (asymmetric, **g**) hBN terraces, with the incidence of zeroth-order hyperbolic polaritons at the black dashed lines. The green boxes denote the locations of the simple slab hBN and the step-shaped hBN terraces in our simulations. In the simple slab edge (**e**), the left side is extended to infinity. In the step-shape edge (**g**), both sides are extended infinitely. **f**, **h,** FT spectra of the reflected fields in (**e**) and (**g**), respectively. The momenta k_l' of various-order hyperbolic polaritons agree well with our experimental results in Figure 2. The arrows mark the polariton modes at different branches. **i**, **j,** 3D bar graphs of reflectivity R_{ij}: the energy ratio between the reflected j-th order mode due to the incident i-th order mode from hBN terraces featuring the simple slab and step-shape edges, respectively.
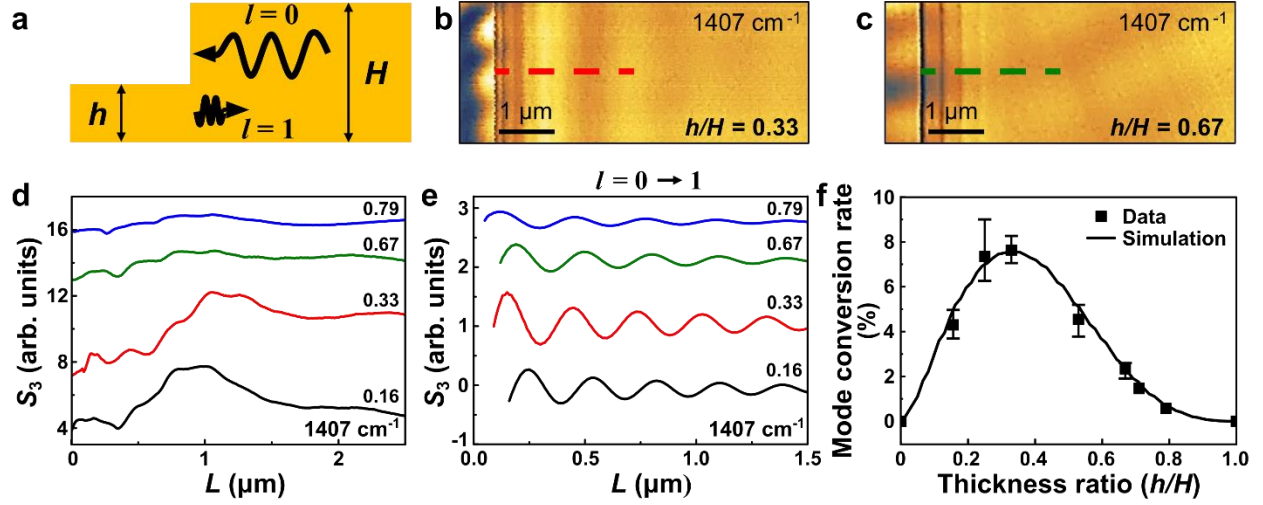
Figure 5 | Altering hyperbolic polariton mode conversion by varying the step size. a, The schematic of the hBN terrace featuring a step-shape edge. h and H indicate the thinner and thicker sides of the hBN, respectively. **b**, **c,** Representative s-SNOM images of step-shape edges with thinner side thicknesses h = 17 and 34 nm (h/H = 0.33 and 0.67). s-SNOM line profiles (**c**) are obtained from red and dark green dashed lines. **d**, s-SNOM line profiles over step-shaped edges with h/H = 0.16, 0.33, 0.67, and 0.79. **e,** Converted $l = 0 \rightarrow 1$ polariton profiles taken from the inverse FT of the s-SNOM line profiles in (**d**). **f**, The dependence of the mode conversion rate R_{01} on the step ratio h/H. The thickness of the thicker side is H = 51 nm. Error bars represent the observed range (minimum–maximum) of mode conversion rates.

Editor Summary:
High-order modes of hyperbolic polaritons – hybrid light-matter interactions – in anisotropic van der Waals materials hold potential for nanophotonics applications. Here, the authors report the observation of polariton mode conversion in step-shaped terraces of hexagonal boron nitride and α-MoO3.

Peer Review Information:
Nature Communications thanks Guanyu Lu and the other, anonymous, reviewer(s) for their contribution to the peer review of this work. A peer review file is available.